-RESEARCH PAPER-

International Journal of Mining and Geo-Engineering

IJMGE

IJMGE 56-1 (2022) 33-39

DOI: 10.22059/IJMGE.2021.276870.594786

Determination of alteration genesis and quantitative relationship between alteration and geochemical anomaly using support vector machines

Hossein Mahdiyanfar [a, *], Mojtaba Mohammadpoor [b], Maryam Mahdavi [b]

[a] *Department of mining engineering, University of Gonabad, Gonabad, Iran*

[b] *School of Mining Engineering, College of Engineering, University of Tehran, Tehran, Iran*

Article History:

Received: 26 February 2019.

Revised: 14 June 2021.

Accepted: 17 June 2021.

ABSTRACT

In this research, a support vector machine (SVM) as a supervised classification method has been used to explore the relationship between the geochemical anomaly and the surface alterations quantitatively in the Tanurcheh mineralization area. The Tanurcheh area has been located in the Khorasan Razavi province, Iran. This area has been considered as a high potential region for Cu and Au mineralization. The different mineralization processes of Au and Cu have unclearly been intertwined in this area and have created extreme surface alterations.

Determination of the major origin of mineralization that has created strong alterations in this area is an important issue that can be addressed using a new proposed scenario. The relationship between the geochemical distribution map and the alteration zone was mathematically calculated using the proposed approach and then the geochemical anomaly map was predicted based on the alteration zones as an innovative achievement.

In this paper, the Au and Cu geochemical data were divided into three classes, namely background, regional anomaly, and local anomaly using the probability plot method. Two threshold values for Cu (70 and 300 PPM) and Au (0.13 and 0.4 PPM) were obtained by the probability plot method. Then the SVM was utilized to classify the geochemical samples using the ASTER images based on these obtained thresholds. The ASTER 14-band images were used as features in this classification. Using this novel scenario, the relationships between the Au and Cu mineralization processes with the intensity of alterations were determined and therefore the origin of these alteration zones was clarified. The SVM classification indices of correct classification rate (CCR) and confusion matrix demonstrate the main origin of alterations is related to the Cu mineralization process in this area. The CCR indices obtained based on the Au and Cu thresholds are 0.66 and 0.85 respectively. It demonstrates the intensity of alterations has more been affected by the Cu mineralization process and there is a relatively good relationship between the alteration zone and the Cu geochemical distribution map. Finally, the geochemical anomaly and background maps were properly predicted using the SVM and the ASTER bands. This paper shows the new application of SVM as a powerful tool for the interpretation of geochemical anomalies and the intensity of alteration.

Keywords: *Anomaly separation, ASTER images, Geochemical data, Pattern recognition, Support vector machine*

1. Introduction

The geochemical anomalies and alteration zones can have a high relationship together in the hydrothermal mineralization areas. The major aim of this research is to evaluate the relationship between the geochemical distribution map and ASTER satellite images mathematically using the SVM. Using this scenario, the geochemical anomaly map can be predicted by the ASTER images and alteration intensity. Up to now, the geochemical mapping has been just performed using common geochemical methods such as fractal and statistical techniques, and the relationship between the geochemical anomaly map and alteration intensity has not been studied mathematically. The application of machine learning in the interpretation of geochemical data is an important topic in mining geochemistry. Zuo (2017) investigated the advantages and disadvantages of machine learning for geochemical purposes. Machine learning can be used for interpreting the complicated geochemical distribution maps and detecting the meaningful geochemical associations in mining exploration and environmental pollutions. Machine learning can play an important role in this way shortly. Machine learning as a powerful technique has not been widely used for geochemical mapping [1]. Various machine learning methods have been performed for interpreting the geochemical data and identifying the geochemical anomaly [2-9].

The SVM as a supervised classification approach is one of the best techniques due to its ability in minimizing the prediction error and the model complexity, simultaneously [10, 11], and has recently been used for mineral prospectively mapping [1]. The SVM can be trained and then predict the complicated patterns concealed in the dataset and extract useful information without considering the data distribution. Therefore, SVM has been widely applied for various aims in mining exploration such as classification and pattern recognition [1].

Twarakavi et al. (2006) performed the SVM for mapping of arsenic concentration using gold concentration [12]. Chen and Wu (2017) applied the SVM as a useful tool for determining the multivariate geochemical anomalies in the stream sediment data [8].

The geochemical mapping as valuable progress in mineral exploration is commonly performed using the spatial interpolation of

* Corresponding author. Te: +98-5157229802, *E-mail address:* hssn.shahi@gmail.com (H. Mahdiyanfar).

element concentrations. The past applications of SVM for geochemical mapping have only been based on geochemical data. In this research, a novel approach was proposed based on the SVM for identifying the relationship between the geochemical anomaly and ASTER images in the Tanurcheh mineralization area.

In this study, the SVM has been applied for the identification of the genesis of mineralization and determination of the role of Au and Cu mineralizations on the intensity of alterations. In continuation, the mineralization processes that create the alteration zones have been discussed based on the results of SVM and the geochemical map has been delineated based on the ASTER images.

2. Case study

The studied area covers the ASTER edge of the 1:100,000 scale geological map of Feyzabad, which is located on the Khaf-Daruneh geological belt. At the north of the Daruneh fault, the Taknar zone has been uplifted in the form of a wedge-shaped block consisting of various lithological units. The Tertiary volcanic activities between the Daruneh and Taknar faults consist of the dark-gray tuffs and in some places ignimbrite at the beginning with black lava flows that have an andesitic composition in their continuance. Thick units of white brecciated tuffs, volcanic breccias, sandy tuffs, ignimbrite, and lapilli-tuff cover the first sequence. The Post-Eocene magmatism in the north and central parts of the Feyzabad area is observed in the form of granodiorite and diorite intrusions within the Neocene volcanic and pyroclastic rocks [13]. The geological map and the location of the Tanurcheh area are shown in Figure 1.

There is some important mineralogical evidence of gold and copper in the Tanurcheh exploration area. The hydrothermal alteration system has been extended in an area with 4km² within the volcanic host rocks and has been covered with alluvial sediments at the northern part. The oxidizing and leaching intensity in the surface rocks is recognized by weathering of finely disseminated pyrite crystals and the remainders of other sulfide minerals that can be observed in different parts of the exploration area. The strong quartz-sericite alteration that is mostly within the outcrops of intrusive porphyry bodies contains the quartz in their texture and is located at the central part of the exploration area. Local evidence of hydrothermal breccia and veinlets having silica and box-works of iron oxides are the result of the weathering of primary iron and copper sulfides [13].

The majority of rocks in the alteration zone are volcanic with various textures and chemical compositions that are massive or layered, dipping northward. The most significant intrusive body in the area recognized through field studies is the stock quartz-porphyry mass. These masses are the first targets for gold-copper mineralization. These rocks have been composed of rounded and large-sized quartz, altered biotite (primary), and tabular feldspar in a fine-grained silica matrix, also with evidence of demolished pyrite in the texture. The texture of sulfide mineralization is mainly disseminated and in some places is in the form of veinlets within intrusive porphyry stocks and their surrounding rocks. The sulfide mineralization appears in most cases as pyrite and in some cases as chalcopyrite at the southeast parts and also the western edge of the alteration system. Pyrite has usually been oxidized to secondary limonite and rarely to Jarosite. At the central part of the alteration system, the acid leaching zone can be recognized by box-work textures related to the complete leaching of sulfide minerals such as pyrite. The veinlets of stock-work, semi-parallel veinlets with secondary iron oxides at the margins, have been located within the phyllic alteration zone. Secondary iron oxides such as hematite, goethite, and limonite that have been distributed over the altered area can result from the oxidization of sulfide minerals such as pyrite and chalcopyrite [13].

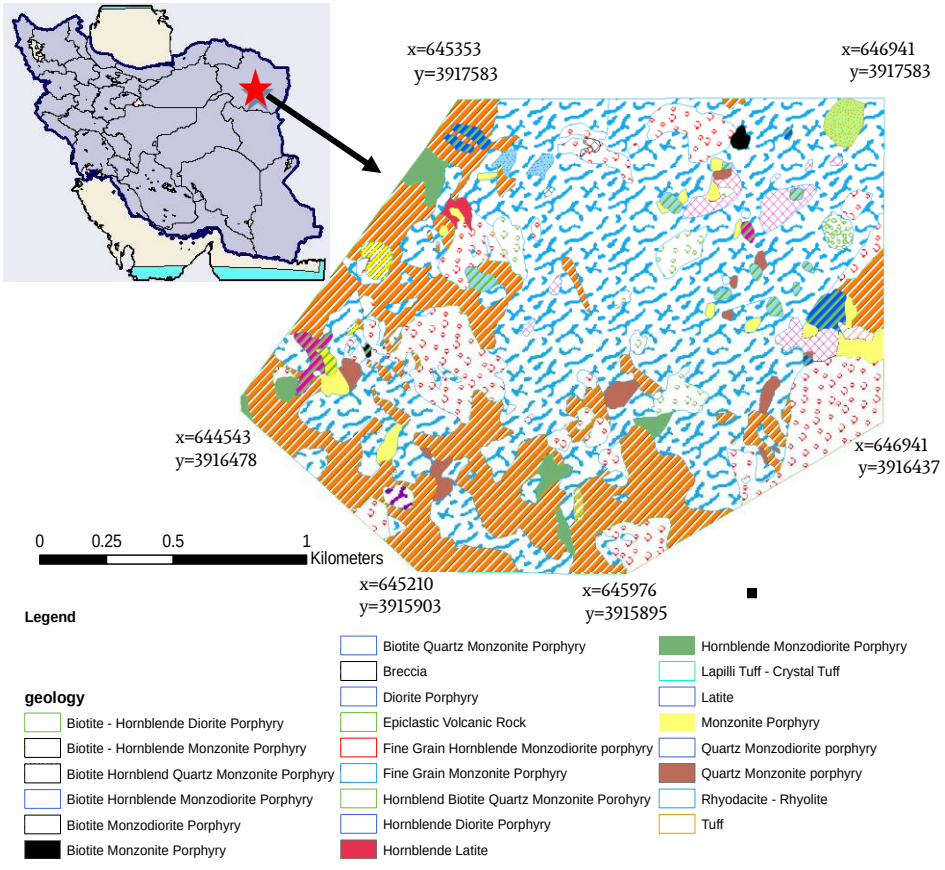

Figure. 1: The geological map of Tanurcheh mineralization area

3. Material and methods

3.1. Geochemical sampling and ASTER images

93 scattered rock and soil samples from mineralization outcrops of sulfide, secondary iron oxides, silica ± iron oxides veinlets, and alteration zones as the main part of Tanurcheh area were selected and analyzed using inductively coupled plasma mass spectrometry (ICP-MS) method for detecting 45 elements such as Au, Cu, Ag, As, Mo, etc. The locations of these samples and the ASTER image in the study area have been illustrated in Figure 2.

The ASTER images provide remote sensing data in the 14 spectral bands. The detailed descriptions of any pixels in the 14 bands of ASTER images are achievable. In this mineralization area, the 14 bands of ASTER were used as features for the geochemical samples in the SVM classification. Data acquisition (detailed descriptions of pixels in the locations of geochemical samples) from these bands was performed by MATLAB and GIS software. These achieved data were stored in a matrix. A sample of the dataset matrix is shown in Table1. The SVM classification was applied to this matrix. This matrix provides the geochemical samples and their features in the 14 bands of ASTER.

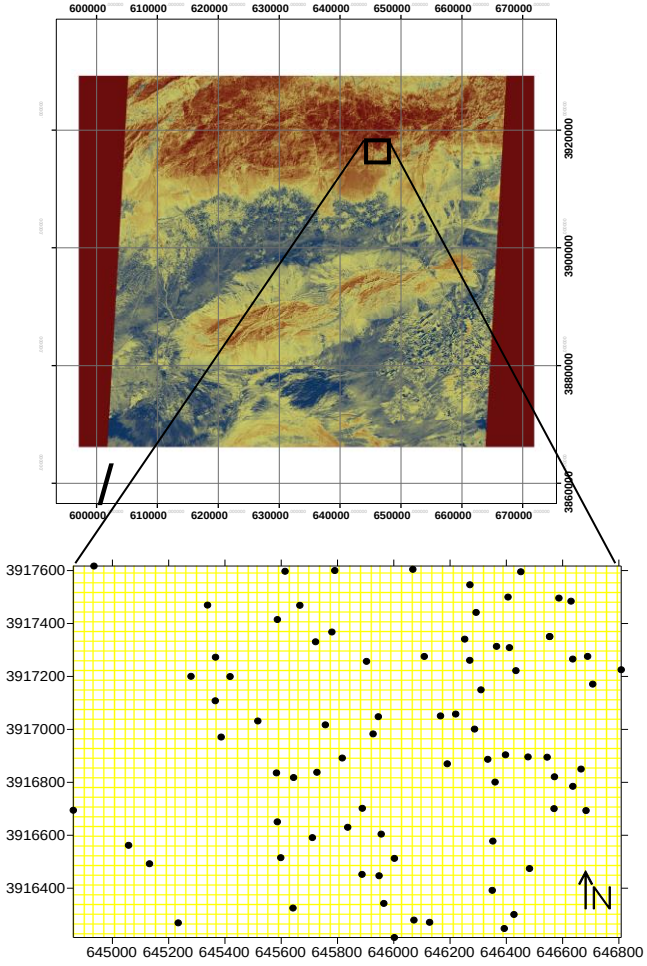

Figure. 2: The location of geochemical samples and ASTER satellite imagery in the study area

3.2. Support vector machine (SVM)

SVM, as a supervised non-parametric statistical classifier, is useful for the classification of remote sensing data [14]. SVM applies a cloud to split the data of two groups from each other so that the hyperplane has the maximum distance from each side to both groups. The closest examples to this page are called vectors, as shown in Figure 3. These specimens specify some sort of boundary of their group [15]. SVM in the simplest form, the linear SVM, consists of a hyperplane that separates the set of positive and negative samples with maximum distance (figure3).

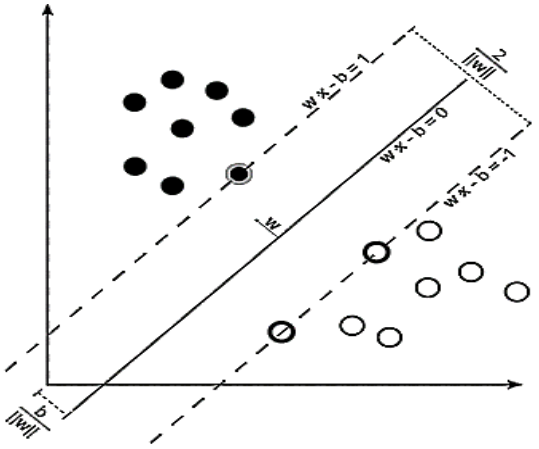

Figure. 3: An illustration of the classification of SVM that divides the samples into superficial groups. The support pages are specified as a dashed line and the distance between the two screens is |W|/2 [15]

Table 1: A sample of data set: the geochemical samples and their features obtained from the ASTER images were used for the SVM classification

Geochemical data			Features for SVM classification (Data acquisition from the ASTER image)			
samples	Cu assay	Geochemical class	Band1	Band2	Band13	Band14
1	65	B	160	23	42	200
2	38	B	20	99	40	110
3	120	RA	140	210	179	28
4	410	LA	200	140	45	67
5	320	LA	12	55	37	120

Assume that for the classification of data with m training sample $[(x_1, y_1),(x_m, y_m)]$ with the label of the group $y_i \in [-1,+1]$, the aim is to find the linear differentiation function $w \cdot \Phi(x) + b = 0$, which separates the two groups based on the mapping of the input space, where Φ is the linear mapping operator. The following problem is defined for the production of optimal hyperplanes with the maximum possible margin and minimum error in the training of linear SVM:

$$\min_{w,b} \frac{1}{2}\| w \|^2 + C \sum_{i=1}^{m} \xi_i \quad \min_{w,b} \frac{1}{2}\| w \|^2 + C \sum_{i=1}^{m} \xi_i \tag{1}$$

$$subjecttoy_i\,(w \cdot \Phi(x) + b) \geq 1 - \xi_i\,,\ \xi_i \geq 0 \tag{2}$$

Considering the increase of the hyperplane margin for the least error in network learning by data, variable C is included in the relationship that creates the compromises between margin increase and the least error in network learning. For this reason, when a linear mapping cannot prevent the collision of samples, coefficient C is determined to increase the edge of the margin by decreasing the network learning error [16]. The following equation can be solved using Lagrange coefficients:

$$\max_{\alpha} \sum_{i=1}^{m} \alpha_i - \frac{1}{2}\sum_{i,j=1}^{m} \alpha_i \alpha_j y_i y_j k(x_i, x_j) \tag{3}$$

$$w = \sum_{i=1}^{m} \alpha_i y_i \phi(x_i), \quad \sum_{i=1}^{m} \alpha_i y_i = 0, \quad 0 \leq \alpha_i \leq C \tag{4}$$

In the training step, each pixel of a learning set is assigned by a class tag. The training algorithm tries to find the optimal separation hyperplane that maximizes the margin between the nearest pixels [17]. The boundary pixels, called support vectors, are used to create a decision surface. In the prediction step, each unlabeled pixel receives a label

based on the relative distance to the hyperplane. The kernel function can separate the datasets that are nonlinear to be detected in the feature space [18]. The decision function is given by:

$$Lbl(x) = sign\left(\sum_{i=1}^{N}(a_i * b_i * K(x_i, x) + b)\right) \quad (5)$$

Where x is the input pixel vector, x_i is the *ith* support vector, N is the number of support vectors, a_i and y_i is the *ith* coefficients of Lagrange and the corresponding classification tag, respectively, and finally, b is the decision shift coefficient. K is a kernel function used to convert the original data to the feature space [19]. Different kernels can be used in the SVM such as linear, polynomial, and Gaussian (RBF). The RBF kernel can be defined as:

$$K(x_i, x) = exp\ (-\gamma * \| x\_i - x \|^2) \quad (6)$$

Where γ is the RBF coefficient, determined after scanning the data, x is the input pixel vector, and x_i is the *ith* support-vector. In this study, the ASTER pixels have been considered as test and train data based on the location of geochemical background, anomaly, and high anomaly.

4. Results and Discussion

The interpretation of geochemical data is an important subject in mining exploration. The descriptive statistical characteristics of original geochemical data in this mineralization area are shown in Table 2.

The geochemical migration of elements and alteration of host or country rocks can occur during the mineralization process. There is an interesting relationship between the geochemical anomaly map and alteration zone in most mineralization areas. Until now, this relationship has not been studied mathematically. In this paper, the relationship between the geochemical background (B), regional anomaly (RA), and local anomaly (LA) classes and alteration zone has mathematically been studied using the SVM. The meaningful relationship between the anomaly map and alteration map demonstrates that their genesis and origins are similar together. There are two different mineralization processes of Cu porphyry and Au veiny mineralization in the Tanurcheh area that have unclearly been intertwined and have created extreme surface alterations [20, 21]. Determination of the major mineralization origin of these strong alterations is an important issue in this area. For this aim, the below steps for the new proposed scenario have been performed. The schematic map of these steps has been illustrated in Figure 4.

The applied steps in this new approach are as bellow:

1- Determining the thresholds of geochemical anomaly and background for Cu and Au geochemical data using probability plot method:

Three classes consisting of B, RA, and LA were extracted from the geochemical data. The thresholds of 70 and 300 (PPM) divided the Cu grades into B, RA, and LA classes. Three classes of B, RA and LA for Au elements were also obtained based on the thresholds of 0.13 and 0.4 (PPM). The statistical characteristics of these classes are shown in Table3.

2- Plotting the geochemical samples on the ASTER image in the GIS environment and acquiring the data in MATLAB:

The surface geochemical samples were plotted on the ASTER image in the GIS and the characteristics of 14 ASTER bands for any geochemical samples were extracted using GIS and MATLAB software. These features are reflection values of these pixels in the 14 bands. Therefore, after this step, 14 features for any geochemical samples are obtained from the ASTER images. We applied image processing methods on the ASTER images for data mining and a matrix consisting of 93 rows (geochemical samples) and 14 columns (the features of 14 bands) was obtained. The geochemical samples in these rows were divided into three classes of B, RA, and LA-based on the obtained thresholds in step1.

3- Classifying the geochemical samples based on the 14 obtained features using the SVM:

The 93 geochemical samples containing 14 features were considered as test and train data. The SVM method was applied for the classification of these geochemical samples based on the three classes of geochemical B, RA, and LA. Therefore, the ASTER 14-bands images that cover this area were applied as features for the SVM classification. The classification process of SVM was accomplished for Au and Cu separately.

The SVM classified the geochemical samples in three classes of B, RA, and LA for Cu and Au separately based on the 14 features of ASTER images. Tables 4 and 5 show the obtained confusion matrixes using the SVM based on the Au and Cu geochemical classes. These matrixes illustrate that 94%, 39%, and 67% of B, RA, and LA geochemical samples have been correctly classified based on the Au thresholds. The classification of geochemical samples based on the 14 bands using Cu thresholds provides better results (Table 5). The accuracy values based on the Cu geochemical B, RA, and LA classes are 96%, 62%, and 97%, respectively. It means that 96.6% of Cu local geochemical anomaly samples were correctly classified and distinguished using the 14 features of ASTER images and 96% of samples that are in the background area were properly detected. This scenario mathematically demonstrates the geochemical anomaly and background can be predicted using the ASTER images and alteration zone and there is an interesting relationship between the geochemical distribution map and alteration zone. It is a new achievement in mathematical geosciences

5- Determination of the major origin of alterations using quantitative indices and prediction of Cu geochemical anomaly map based on the ASTER images:

Table 2: The descriptive statistical analysis of original geochemical data

	mean	median	max	min	standard deviation	variance	skewness	kurtosis
Cu	80.7	44	561	5	106	11241	2.92	9.949
Au	0.19	0.07	1.1	0.007	0.25	0.065	1.977	3.408
Mo	16.99	9	196	1	25.35	642.7814	4.261	24.053
Pb	537.63	58.5	7354	4	1175	1380882	3.446	13.47
Zn	106.4	38	1070	1.67	170	28938	2.8774	10.081

Table 3: The statistical characteristics of background (B), regional anomaly (RA), and local anomaly (LA) classes

	class	average	Standard deviation	minimum	maximum
Cu	B (Assay<70ppm)	28	17	5	68
	RA (70ppm<Assay<300ppm)	137	47	70	234
	LA (300 ppm<Assay)	488	104	336	561
Au	B (Assay<0.13ppm)	0.45	0.032	0	0.13
	RA (0.13ppm< Assay<0.4ppm)	0.2	0.063	0.14	0.39
	LA (0.4 ppm<Assay)	0.66	0.23	0.41	1.1

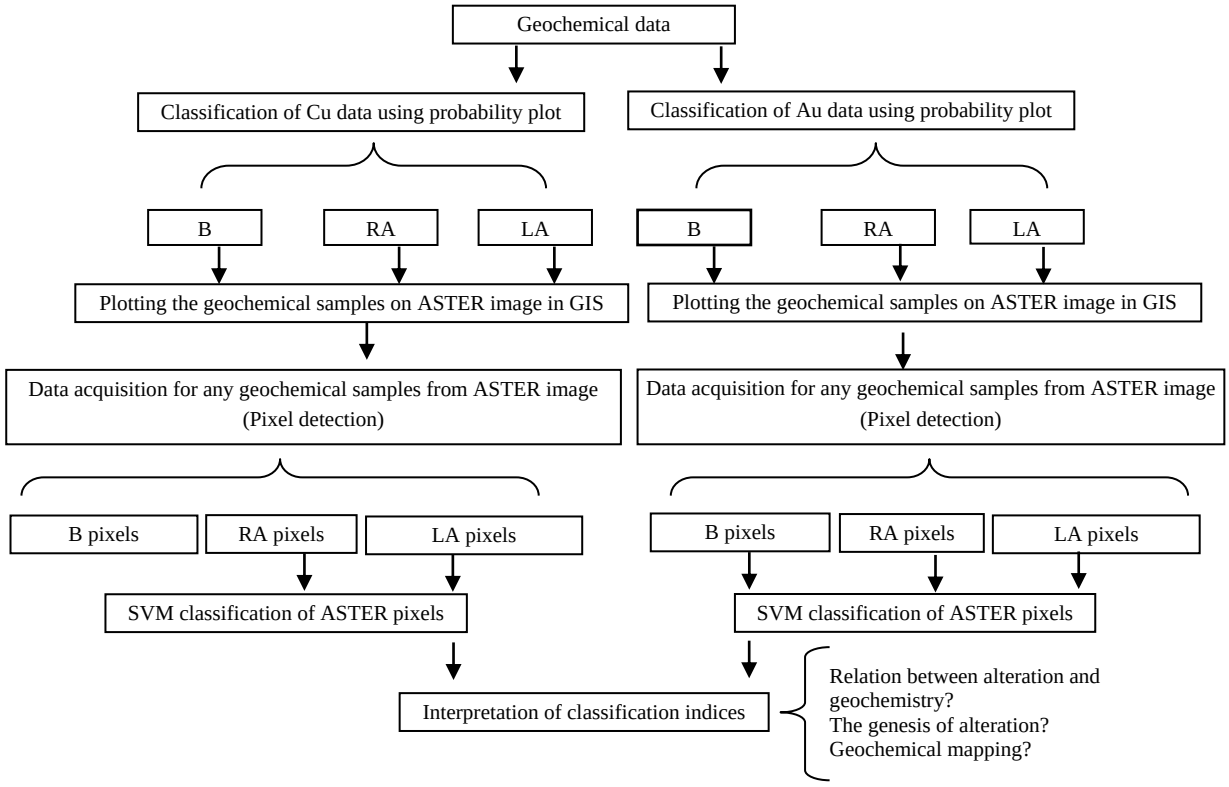

Figure. 4: The schematic map of various steps in the proposed approach

Table 4: The confusion matrix obtained from the SVM classification of geochemical samples based on the ASTER images and Au background (B), regional anomaly (RA), and local anomaly (LA) classes

		predicted classes		
		B	RA	LA
Real Classes	B	0.939103	0.022436	0.038462
	RA	0.551323	0.392328	0.056349
	LA	0.325	0	0.675

Table 5: The confusion matrix obtained from the SVM classification of geochemical samples using ASTER images and Cu background (B), regional anomaly (RA), and local anomaly (LA) classes

		predicted classes		
		B	RA	LA
Real Classes	B	0.960402	0.037111	0.002488
	RA	0.374074	0.625926	0
	LA	0	0.033333	0.966667

In this step, the accuracy indices of SVM classification on Au and Cu elements are evaluated. Fawcett (2003) discussed some accuracy indices for the evaluation of classifier performance [22]. The accuracy indices of SVM classifications were derived from the obtained confusion matrixes. The indices of true positive rate (TP), false positive rate (FP), predictive power (PP), and correct classification rate (CCR) are calculated as bellow equations [22, 23]:

$$True\ positive\ rate = \frac{positives\ correctly\ classified}{total\ positives} \quad (7)$$

$$False\ positive\ rate = \frac{negatives\ incorrectly\ classified}{total\ negatives} \quad (8)$$

$$pp = \frac{(True\ positive\ classified)}{(False\ positive\ classified)} \quad (9)$$

$$CCR = \frac{sumation\ of\ odiagonal\ elements^{(Correctly\ classified)}}{(numbers\ of\ classes)} \quad (10)$$

The samples that are correctly classified are named "positive correctly classified samples" and the samples that are incorrectly classified in the other classes are named "negative incorrectly classified samples". These obtained indices are shown in Table 6.

The classification performance indices for two SVM classifiers based on the Au and Cu elements have been delineated and compared together in Figure 5. The CCR as an important criterion is calculated by the average of diagonal elements in the confusion matrix. The performance indices of the Cu element generally show more high values than the Au element. The CCR values of Cu and Au elements as important indices are 0.85 and 0.66, respectively. The SVM method based on the Cu thresholds shows a relatively high CCR.

Table 6: The classification performance indices have been calculated based on the confusion matrixes

Index	**Cu**			**Au**		
	B	RA	LA	B	RA	LA
True Positive Rate	0.72	0.9	0.99	0.52	0.95	0.88
False Positive rate	0.02	0.16	0.016	0.05	0.235	0.146
Correct Classification Rate		0.85			0.66	

One of the performance criteria is relative operating characteristic (ROC). The ROC curve shows the variation of TP and FP in a diagram [22]. In this graph, the X and Y axes are related to the FP and TP, respectively. The ROC graph for Au and Cu elements has been depicted in Figure 6. The upper left corner point with the coordinate of (0, 1) shows the best classification. The performance of classification is related to the distance of points to this corner. The ROC diagram also shows a more performance for Cu rather than Au in this classification.

The local geochemical anomaly samples for Cu mineralization (LA-Cu) have more perfect performance and the background samples based on the Au assay (B-Au) show the least performance in this diagram.

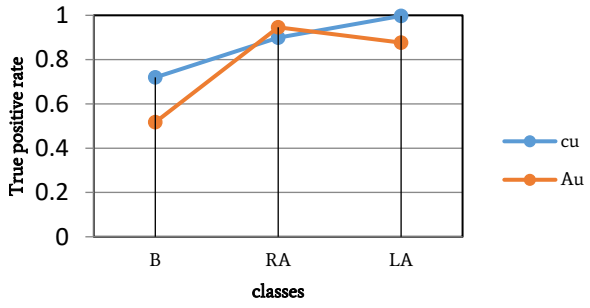

Figure 5: Comparison of predictive power indices of SVM for Au and Cu elements

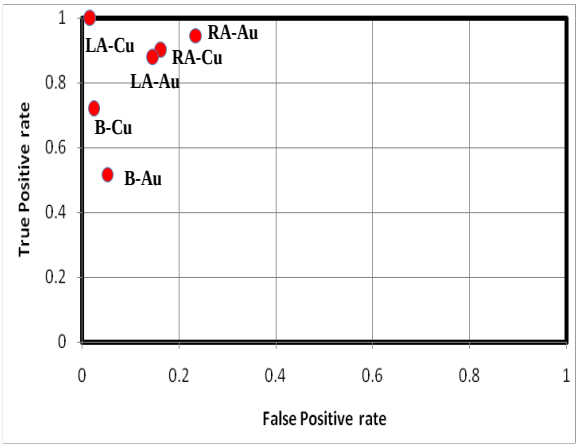

Figure 6: The ROC graph for B, RA, and LA in the Au and Cu classification

The obtained performance and accuracy indices of SVM show better results for Cu mineralization and the geochemical background and anomaly samples based on the Cu assays can be properly predicted by the features of ASTER images. Therefore, there is a more effective relationship between the Cu mineralization process and the alteration zone. The comparison of the performance of SVM classification based on the Au and Cu geochemical data demonstrates the Tanurcheh alteration zone is more affected by the Cu mineralization process than the Au mineralization. The calculated accuracy indices demonstrate there is an interesting relationship between the alteration and Cu geochemical distribution map in this mineralization area. The geological information and the alteration types in the study area show a probable porphyry Cu mineralization that is associated with the Au veiny mineralization. The SVM results are properly confirmed by the exploratory information and suspected mineralization types in the area. This research demonstrates that there are significant relationships between the surface geochemical anomaly and alteration zones in mineralization and non-mineralization areas that are achievable using advanced pattern recognition methods.

In the next step, the Cu geochemical map consisting of B, RA, and LA areas were predicted using the ASTER14 bands' data (Figure 7). The 96.7% of local anomaly samples, 62% of regional anomaly samples, and 96% of background samples have been correctly predicted using the ASTER images. In this Fgure, the locations of samples and mineralization veins have also been illustrated. There is interesting conformity between the anomaly areas and the mineralization veins that shows the high potential of this classification method for Cu anomaly separation.

The SVM classification on the ASTER images distinguished an NW-SE trend for Cu anomaly that is associated with mineralization veins. The Cu geochemical distribution map obtained from the original geochemical data has also been depicted in Figures 8 and 9. These maps also show a high resemblance to the Cu distribution map of the SVM classifier.

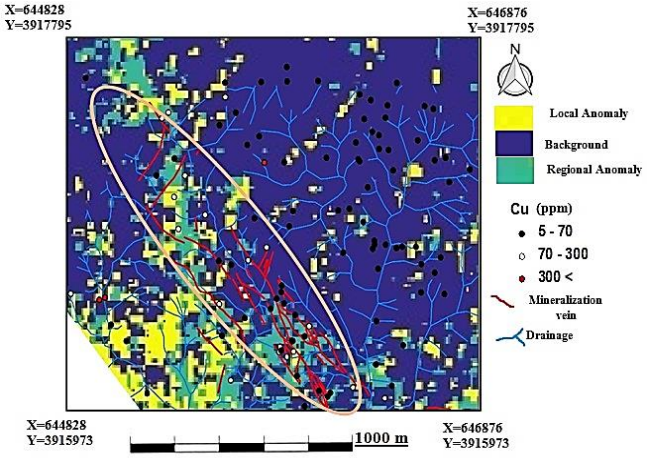

Figure 7: The predicted Cu geochemical anomaly map using the SVM and ASTER images

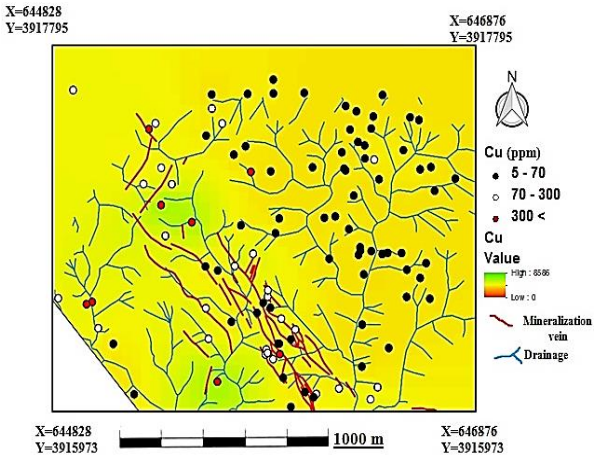

Figure 8: The Cu geochemical distribution map obtained from the original geochemical data

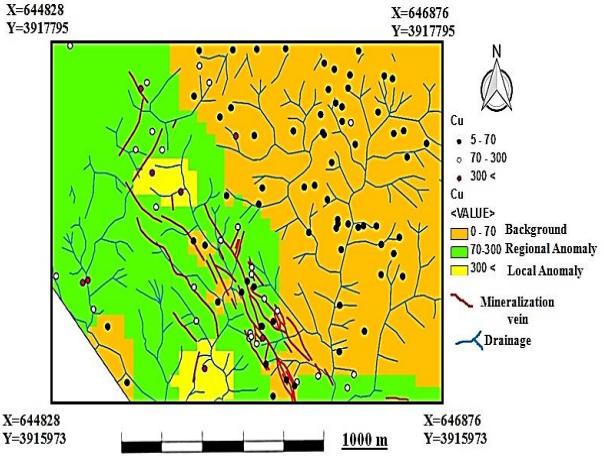

Figure 9: The Cu classified geochemical distribution map obtained from the original geochemical data

Identification of various mineralization processes and their effects on alteration zones is an important achievement in mining exploration. The results of this study indicate the capability of SVM for the determination of the original genesis of alteration zones mathematically. The application of SVM and ASTER images is a useful idea for geochemical prospectivity mapping.

5. Conclusion

This research presents the novel application of the SVM classifier for anomaly mapping and detecting the relationship between the Au and Cu geochemical distribution map and alteration zones in the Tanurcheh Cu-Au mineralization area. In this area, detecting the major origin of the large and strong alterations is an important issue especially since we are faced with two different mineralization processes of Cu porphyry and Au veiny mineralizations. In this study, the SVM was used to classify the 93 geochemical samples as a testing and training dataset to three classes of background, regional anomaly, and local anomaly that were obtained using the probability plot method for Cu and Au elements, separately. In these classifications, the ASTER 14-band images were applied as features for these samples. The SVM computationally detected the relationship between the Cu and Au geochemical classes and the alteration zones. The CCR values of SVM classifiers for Cu and Au elements are 0.85 and 0.66, respectively. The geochemical samples in the local anomaly, regional anomaly, and background were classified with accuracy values of 97%, 62%, and 96%for Cu and 67%, 39%, and 94% for Au, respectively. The performance indices of SVM showed better results for Cu porphyry than Au veiny mineralization type. The SVM showed the alteration zones are properly related to the Cu geochemical distribution map and have more been affected by the Cu porphyry mineralization type than the Au veiny mineralization. Finally, the Cu anomaly map was properly predicted using the ASTER images and SVM classifier.

Acknowledgments

We would like to thank Zarmehr Company for providing access to the database.

REFERENCES

[1] Zuo, R.(2017). Machine Learning of Mineralization-Related Geochemical Anomalies: A Review of Potential Methods, Natural Resources Research

[2] Chen, Y., Lu, L., & Li, X. (2014). Application of continuous restricted Boltzmann machine to identify multivariate geochemical anomaly. Journal of Geochemical Exploration, 140, 56–63.

[3] O'Brien, J. J., Spry, P. G., Nettleton, D., Xu, R., &Teale, G. S. (2015). Using random forests to distinguish gahnite compositions as an exploration guide to Broken Hill-type Pb–Zn–Ag deposits in the Broken Hill domain, Australia. Journal of Geochemical Exploration, 49, 74–86.

[4] Gonbadi, A. B., Tabatabaei, S. H., & Carranza, E. J. M. (2015). Supervised geochemical anomaly detection by pattern recognition. Journal of Geochemical Exploration, 157, 81–91.

[5] Kirkwood, C., Cave, M., Beamish, D., Grebby, S., & Ferreira, A. (2016). A machine learning approach to geochemical mapping. Journal of Geochemical Exploration, 167, 49–61.

[6] Zhao, J., Chen, S., &Zuo, R. (2016). Identifying geochemical anomalies associated with Au–Cu mineralization using multifractal and artificial neural network models in the Ningqiang district, Shaanxi, China. Journal of Geochemical Exploration, 164, 54–64.

[7] Xiong, Y., Zuo, R. (2016). Recognition of geochemical anomalies using a deep autoencoder network. Computers & Geosciences, 86, 75–82.

[8] Chen, Y., & Wu, W. (2017). Application of one-class support vector machine to quickly identify multivariate anomalies from geochemical exploration data. Geochemistry: Exploration, Environment, Analysis, 17, 231–238.

[9] Zuo, R. and Xiong, Y. (2017). Big Data Analytics of Identifying Geochemical Anomalies Supported by Machine Learning Methods. Natural Resources Research, pp.1-9.

[10] Vapnik, V. (1995). The Nature of Statistical Learning Theory: Springer, New York, 314 p.

[11] Vapnik, V. (1998). Statistical Learning Theory: Wiley, New York, 736 p.

[12] Twarakavi, N. K. C., Misra, D., &Bandopadhyay, S. (2006). Prediction of arsenic in bedrock-derived stream sediments at a gold mine site under conditions of sparse data. Natural Resources Research, 15, 15–26.

[13] Zarmehr Company, (2004). exploration report of Tnurcheh Au –Cu mineralization area.

[14] Salimi, A., Ziaii, M., HosseinjaniZadeh, M., Amiri, A. and Karimpouli, S. (2015). High performance of the support vector machine in classifying hyperspectral data using a limited dataset. Int. Journal of Mining & Geo-Engineering, 49(2), pp.253-268.

[15] Lu, J., & Zhang, E. (2007). Gait recognition for human identification based on ICA and fuzzy SVM through multiple views fusion. Pattern Recognition Letters, 28(16), 2401-2411.

[16] Thodoridis, S and Koutroumbas, K (2009) "Pattern recognition", Fourth Edition, Elsevier.

[17] Wu, Y., Yang, X., Plaza, A., Qiao, F.,Gao, L., Zhang, B., and Cui, Y. (2016). Approximate Computing of Remotely Sensed Data: SVM Hyperspectral Image Classification as a Case Study. IEEE Journal of Selected Topics in Applied Earth Observations and Remote Sensing, 9(12), pp.5806-5818.

[18] Chang, C. (2007). Hyperspectral Data Exploitation, Theory, and Applications. Published by John Wiley & Sons, Inc., Hoboken, New Jersey.

[19] Camps-Valls, G. and Bruzzone, L.(2005). Kernel-based methods for hyperspectral image classification. IEEE Transactions on Geoscience and Remote Sensing, 43(6), pp.1351-1362.

[20] Mahdiyanfar, H. (2020). Prediction of economic potential of deep blind mineralization by Fourier transform of a geochemical dataset. Periodico di Mineralogia, 90(1).

[21] Mahdiyanfar, H. (2020). Identification of deep blind mineralization and dispersed zones using geochemical frequency anomaly in comparison with Zonality method. Journal of Analytical and Numerical Methods in Mining Engineering, 10(23), 1-16.

[22] Fawcett, T. (2003). Notes and Practical Considerations for Data Mining Researchers, Intelligent enterprise Technologies Laboratory, HP Labs Palo Alto. HPL-2003-4

[23] Swets, J.A. (2014). Signal detection theory and ROC analysis in psychology and diagnostics: Collected papers. Psychology Press.